HHS Public Access

Author manuscript

Anal Chem. Author manuscript; available in PMC 2017 August 17.

Published in final edited form as:

Anal Chem. 2017 June 20; 89(12): 6358–6366. doi:10.1021/acs.analchem.7b00213.

Implementation of Activated Ion Electron Transfer Dissociation on a quadrupole-Orbitrap-linear ion trap hybrid mass spectrometer

Nicholas M. Riley[1,2], **Michael S. Westphall**[1], **Alexander S. Hebert**[1], and **Joshua J. Coon**[1,2,3,4,*]

[1]Genome Center of Wisconsin, University of Wisconsin-Madison, Madison, WI, 53706, USA

[2]Department of Chemistry, University of Wisconsin-Madison, Madison, WI, 53706, USA

[3]Department of Biomolecular Chemistry, University of Wisconsin-Madison, Madison, WI, 53706, USA

[4]Morgridge Institute for Research, Madison, Wisconsin, USA

Abstract

Using concurrent IR photo-activation during electron transfer dissociation (ETD) reactions, i.e., activated ion ETD (AI-ETD), significantly increases dissociation efficiency resulting in improved overall performance. Here we describe the first implementation of AI-ETD on a quadrupole-Orbitrap-quadrupole linear ion trap (QLT) hybrid MS system (Orbitrap Fusion Lumos) and demonstrate the substantial benefits it offers for peptide characterization. First, we show that AI-ETD can be implemented in a straight-forward manner by fastening the laser and guiding optics to the instrument chassis itself, making alignment with the trapping volume of the QLT simple and robust. We then characterize the performance of AI-ETD using standard peptides in addition to a complex mixtures of tryptic peptides using LC-MS/MS, showing not only that AI-ETD can nearly double the identifications achieved with ETD alone, but also that it outperforms the other available supplemental activation methods (ETcaD and EThcD). Finally, we introduce a new activation scheme called AI-ETD+ that combines AI-ETD in the high pressure cell of the QLT with a short infrared multi-photon dissociation (IRMPD) activation in the low pressure cell. This reaction scheme introduces no addition time to the scan duty cycle but generates MS/MS spectra rich in b/y-type and c/z$^{\bullet}$-type product ions. The extensive generation of fragment ions in AI-ETD+ substantially increases peptide sequence coverage while also improving peptide identifications over all other ETD methods, making it a valuable new tool for hybrid fragmentation approaches.

Graphical abstract

*Corresponding author: jcoon@chem.wisc.edu.

ASSOCIATED CONTENT

Supporting Information

Additional information available in supporting documents, including expanding Materials and Methods descriptions. Raw data and information about identified spectra are available on Chorus (Project ID 1288).

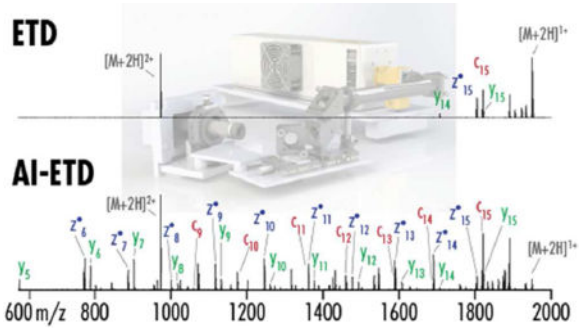

In over a decade of availability on commercial mass spectrometers, electron transfer dissociation (ETD) has become a valuable and ubiquitous fragmentation method used in a wide range of proteomic experiments.[1–6] Continued advancements in ETD instrumentation and methodology have contributed to this sustained utility, and many of these improvements have been incorporated into the newest generation of mass spectrometer (MS) systems. For example, the robustness of the ETD reagent ion sources has been improved,[7] modifications to precursor and reagent ion storage prior to the reactions has improved product ion signal-to-noise (S/N),[8] and calibration routes have standardized ETD reaction times to balance sufficient precursor fragmentation with maximal identification power for proteomic analyses.[9]

Despite these gains, however, a major challenge of ETD remains its reduced dissociation efficiency for precursor ions having low charge density. Low-charge density precursor ions are more compact and often undergo non-dissociative electron transfer (ETnoD), where peptide backbone bond cleavage occurs but fragments are held via together non-covalent interactions.[10–16] ETnoD may impede the generation of sequence-informative product ions and thus limits the utility of ETD in standard shotgun experiments, where the majority of peptide precursors are doubly protonated. That said, ETnoD can be minimized in favor of sequence-informative product ions by supplying the ETD reaction with more energy, and several supplemental activation strategies have been implemented to accomplish this goal. The most ubiquitous approach has been the use of gentle collisional dissociation of ETnoD products, called ETcaD, which is effective at producing more fragmentation and sequence coverage of low charge-density precursors.[17] Likewise, activation of all ETD product ions (including remaining precursor ions, fragment ions, and ETnoD products) with beam-type collisional dissociation, termed EThcD, has proven a valuable way to generate more extensive fragment ion series and sequence information from ETD reactions.[18] For all of their merits, however, ETcaD and EThcD both suffer from fragment ions that have skewed isotope distributions due to hydrogen abstractions[19–21] and, importantly, from increased cycle time due to the secondary activation step after completion of the ETD reaction.

A third alternative to increasing product ion yield in ETD reactions is concurrent infrared photo-activation, *i.e.*, activated ion ETD (AI-ETD). In AI-ETD, IR photons unfold peptide precursor ions by disrupting the non-covalent interactions via slow-heating, increasing product ion yield and the amount of sequence information obtained per spectrum.[22] The concomitant unfolding prevents the pre-existing higher order structure from holding product

ions together after backbone bond cleavage, not only promoting formation of c- and z$^{\bullet}$-type ions but also minimizing the time the product ions are held together to mitigate hydrogen rearrangements that can occur in ETnoD products. We have previously shown that AI-ETD can improve proteome characterization in shotgun experiments and also can increase sequence coverage of intact proteins.[23–25] Notably, AI-ETD accomplishes this without any addition to the standard ETD reaction time, making it highly favorable for high-throughput experiments that look to maximize the number of peptides sequenced per unit time.

The challenge of AI-ETD, of course, is the addition of an IR laser on the mass spectrometer system. Previous implementation of AI-ETD on an Orbitrap system required extensive hardware modifications,[24–26] but the geometry of the newest generation of Orbitrap MS, *i.e.*, the quadrupole-Orbitrap-quadrupole linear ion trap (q-OT-QLT) hybrid,[27] or the Orbitrap Fusion Lumos, enables facile implementation of the laser for robust AI-ETD experiments. Here we describe our straight-forward approach of affixing a continuous wave CO_2 laser to the Lumos system and demonstrate that AI-ETD provides the best performance of all ETD methods for shotgun proteomics. Moreover, we use this implementation of AI-ETD to introduce a new activation scheme called AI-ETD+ that takes advantage of both electron-driven fragmentation and infrared multi-photon dissociation (IRMPD) to generate full sequence coverage of the large majority of peptides identified in LC-MS/MS experiments.

MATERIALS AND METHODS

A quadrupole-Orbitrap-quadrupole linear ion trap (q-OT-QLT) hybrid MS system (Orbitrap Fusion Lumos, Thermo Fisher Scientific, San Jose, CA) was modified to include Firestar T-100 Synrad 60-W CO_2 continuous wave laser (Mukilteo, WA). Four synthetic peptides with the sequences SEDYVDIVQGNR, ENDILVLMESER, ELVNDDEDIDWVQTEK, and INQLISETEAVVTNELEDGR were obtained from New England Peptides (Gardner, MA) and were infused into the mass spectrometer at a flow rate of 5–7 μL/min for analysis with ETD, ETcaD, EThcD, and AI-ETD. LC-MS/MS experiments of tryptic peptides from mouse brain lysates were conducted using 90-minute analyses. Tryptic digestion was performed similarly as described elsewhere.[28–30] Calibrated charge dependent ETD parameters[9] were enabled to determine ETD reagent ion AGC and ETD reaction times for all activation methods, meaning ETD reaction times were the same for a given precursor ion charge state either with and without collisional or photo-activation, and all MS/MS scans utilized the QLT as the mass analyzer with rapid scan speed enabled. Photo-activation for AI-ETD occurred concurrently with ETD reaction, meaning the laser was on only for the duration of the ion-ion reaction time. Tandem mass spectra were searched with the Open Mass Spectrometry Search Algorithm in the COMPASS suite.[31,32] Prior to the search, unreacted precursor peaks, charge reduced precursor peaks, and neutral loss peaks from the charge reduced precursor were cleaned from spectra.[33,34] Product ions searched were c-, z$^{\bullet}$-, and y-type for ETD, ETcaD, and AI-ETD, whereas b-type product ions were included in addition to the other three in searches of EThcD and AI-ETD+ data. Trypsin specificity with three missed cleavages allowed was used and peptide spectral matches (PSMs) were made against the UniProt mouse (mus musculus) database (canonical and isoforms) downloaded on May 12, 2016, which was concatenated with a reversed sequence version of the forward

database. Peptides were filtered to a 1% false discovery rate using both e-value and precursor mass accuracy. See Supplemental Material for more detailed methods.

RESULTS AND DISCUSSION

Instrument modifications

We designed our implementation of the CO_2 laser on a q-OT-QLT system to require minimal additional hardware while still allowing for simple laser installation that maintains alignment integrity and robust instrument performance. Figure 1 illustrates our approach, where we affixed the laser and alignment optics to the instrument chassis itself, removing the need for a laser table and leaving the instrument footprint largely unchanged. Figure 1a shows an overhead view of this setup in relation to the instrument schematic (not to scale), indicating how the laser head is attached to the back of the instrument and the beam is guided into the dual cell linear ion trap using optic mirrors and beam stirrers. Two focusing lenses were also introduced immediately prior to the ZnSe window (25.4 mm in diameter) that was added into the vacuum manifold. The IR photon beam was focused by the first lens to have a waist approximately 1 mm in diameter, and the second lens columnated the beam prior to transmission into the QLT. Figure 1b provides a rendered image of this implementation with appropriate components labeled. The tube housing the lenses makes coarse alignment with the QLT straight-forward and the beam stirrers allow for simple adjustment of fining tuning of the beam position in the x and y dimensions.

By having all laser components fastened to the instrument itself, the alignment remains robust and largely unaffected by small movements that could drastically affect a setup where instrument and laser table are on separate foundations. Additionally, minimizing hardware reduces the costs and space needed to outfit the system with a laser.

The laser was aligned concentric with the QLT for all experiments described in this manuscript using IRMPD fragmentation of background ions as indicators of alignment accuracy. Following the hardware modifications, the Lua instrument control software was modified to trigger the laser to fire when desired using TTL logic and a gate controller. Laser power was controlled using a spare DAC output on the instrument so that power could be adjusted in real time throughout a given experiment. Importantly, the He bath gas pressures used for normal QLT operation remained unchanged for all experiments.

AI-ETD performance

We first assessed our laser-outfitted q-OT-QLT system by dissociating four synthetic tryptic peptides with AI-ETD at various laser powers. For all AI-ETD experiments, the ETD reaction was carried out as normal in the high pressure cell while trapping volume was irradiated only for the duration of the ion-ion reaction with no pre- or post-activation. In this current implementation, laser powers of 12–24 W generally produced the best AI-ETD fragmentation (Figure 2), which is significantly lower than laser powers needed in previous AI-ETD experiments on a linear ion trap-Orbitrap hybrid MS system (Orbitrap Elite) where the pressure in the reaction cell also had to be lowered to achieve optimal AI-ETD

fragmenation.[24,25,35,36] The much shorter laser path and use of focusing optics in this implementation account for this difference, allowing use of lower powered lasers.

Figure 2a displays the intensity of c-, z$^{\bullet}$-, b-, and y-type product ions produced by ETD and AI-ETD at varying laser powers (6–30 W) for the doubly protonated precursor of each of the four peptides. Fragments generated by EThcD and ETcaD are also plotted for comparison, where “nce” denotes normalized collision energy used. For each precursor, intensities of individual fragments are summed for a given fragment ion type, and the intensities of each fragment type are normalized to the greatest value seen for that precursor, allowing for easy comparison across each peptide. Note, a C# script using the C# Mass Spectrometry Library (CSMSL, https://github.com/dbailey chess/CSMSL) was written to extract fragment ions and their intensities. Figure 2b presents the normalized signal (again normalized to the greatest value for each precursor) seen in the c- and z$^{\bullet}$-type fragment ion channels only, i.e., those specific to ETD fragmentation. In both cases, AI-ETD clearly increases fragment ion production over ETD as laser power increases, although over fragmentation can occur. For each peptide, y-type ion generation increases with laser power, but this is not necessarily indication of collisional fragmentation. ETD is known to produce y-type ions in addition to the canonical c- and z$^{\bullet}$-type fragments,[37] so the increase of all three fragment types concomitantly is indicative of improved ETD-like fragmentation. However, increasing b-type ion signal, in addition to degradation of c- and z$^{\bullet}$-type products, at higher laser powers indicates the onset of IRMPD-like fragmentation, which is considered over fragmentation in AI-ETD experiments.

In general, AI-ETD at 18–24 W generated more fragment ion signal than ETD, ETcaD, and EThcD for all four fragment ion types, and AI-ETD always produced the maximum signal for c- and z$^{\bullet}$-type ions. Figure S1 further illustrates the increased conversion efficiency of AI-ETD, displaying the amount of remaining precursor and charge-reduced precursor present in spectra after each activation method. AI-ETD also provided similar improved fragment ion generation for higher charged precursors (z = +3 of INQLISETEAVVTNELEDGR), albeit at lower laser powers (12–18W) for optimal activation, whereas EThcD and ETcaD both decreased total product ion signal compared to ETD (Figure S2).

Increased fragment ion yield with AI-ETD is highlighted in Figure 3a, which shows annotated spectra for ETD and AI-ETD at increasing laser powers for the doubly protonated precursor ion of ENVNDDEDIDWVQTEK. The presence of c-, z$^{\bullet}$-, and y-type in AI-ETD up through 18 W of power is clear, and the presence of b-type ions in the spectrum AI-ETD at 24 W marks the onset of some degree of IRMPD fragmentation as well. This improvement in fragment ion generation is coming directly from unfolding of precursor ions, which mitigates the formation of non-sequence informative ETnoD products, as demonstrated by Figure 3b. Here the isotopic envelopes of the charge-reduce precursor ions are shown for each of the spectra in part a (highlighted in gray in 2a). Monoisotopic m/z peaks of the proton transfer (PTR) and ETnoD products are highlighted in blue and red, respectively. Proton transfer and electron transfer are competing pathways in ETD reactions that vary based on reagent anion used, and a minimal degree of PTR is known to happen with fluoranthene, the reagent used in these experiments.[38–40] If ETnoD were not occurring

at all and PTR was the only contributing factor to the charge-reduced precursor products, the isotope distribution should match the theoretical isotope distribution shown by open white circles.

Clearly, ETnoD products are a major contribution to the charge-reduced precursor products in ETD, but ETnoD products are diminished and ultimately are eliminated as laser power increases with AI-ETD. Note, the isotope distributions are not plotted on the same intensity scale, but the base peak height is given for each. Figure 3c illustrates this concept for other standard peptides, plotting the intensity of the ETnoD (red) and PTR (blue) monoisotopic peaks as a function of laser power. PTR products are largely unchanged by AI-ETD fragmentation (which is expected because PTR is largely a function of reagent), but ETnoD products are greatly reduced at higher AI-ETD laser powers.

With successful implementation of AI-ETD evident from the synthetic peptide studies, we next examined the performance of AI-ETD for shotgun proteomic experiments with 90-minute LC-MS/MS analyses of tryptic peptides from mouse brain lysate. Figure 4 summarizes the results of these experiments, showing how AI-ETD at various laser powers compares to ETD. AI-ETD (18 W) nearly doubled the number of peptide spectral matches (PSMs) as compared to ETD (**panel a**). AI-ETD also improves MS/MS success rate, plotted both as a function of precursor *m/z* (**panel b**) and precursor charge state (*z*) (**panel c**). MS/MS success rate is defined as the number of PSMs successfully sequenced divided by the number of MS/MS scans acquired for a given *m/z* bin or charge state. The significant decline in success rate with ETD for precursors larger that ~600 Th and the low success rates for z = +2 precursors exemplify of ETD's low efficiency with low charge density precursors due to ETnoD. AI-ETD improves success rates across the entire *m/z* range and for all precursor charge states, with the most drastic improvements coming for doubly protonated precursors and high *m/z* ions. Notably, AI-ETD improves MS/MS success rate for all precursor ion charge states, even the $z \geq 3$ precursor ions, where ETD is known to perform well.[10,41] Comparing between AI-ETD laser powers, the lowest power of 12 W does not improve performance as substantially, but the differences between 15 W, 18 W, and 21 W are less significant, with 18 W providing the best overall results.

Introducing AI-ETD+

The main goal of AI-ETD is to augment ETD fragmentation; the onset of substantial collisional dissociation products is considered undesirable. Hybrid fragmentation methods, on the other hand, such as EThcD and ETUVPD (*i.e.*, using ultraviolet photo-dissociation to activate ETD reaction products),[42–44] seek to combine multiple types of fragmentation to generate extensive ion series corresponding to multiple dissociation pathways. This approach has several benefits, including extensive peptide backbone sequence coverage and localization of post-translational modifications (PTMs) that have been demonstrated with EThcD.[18,45–47] Challenges with EThcD and similar hybrid activation methods, however, include both additional time needed to perform both dissociation methods, and loss of sensitivity that can occur during the HCD process (*i.e.*, some degree of product ion signal is lost during HCD fragmentation).

We devised a new hybrid fragmentation approach called AI-ETD+ that combines AI-ETD in the high pressure cell of the dual cell QLT with a short IRMPD activation in the low pressure cell prior to fragment ion mass analysis that occurs in the low pressure trap (see Figure S3 for a sample scan event). The higher bath gas pressures of the high pressure cell (~5 mTorr) are suitable for ETD reactions, but they generally prevent dissociation via IRMPD due to collisional cooling.[48,49] The low pressure cell, however, is used for improved resolution and sensitivity during mass analysis[48] and has low enough pressures (~0.3 mTorr) to perform IRMPD,[49,50] making the shuttling of ions into the low pressure cell standard in QLT operation and presenting an ideal time to perform IRMPD with no additional steps needed in the scan sequence. IRMPD is known to produce b- and y-type ions similar to other collisional activation methods,[51] providing complementary dissociation to AI-ETD. In this scheme, all AI-ETD products are irradiated in the low pressure cell, *i.e.*, no other mass selection occurs prior to the photo-activation, which is similar to EThcD and allows for further fragmentation of the unreacted precursor, a dominant product in all ETD reactions. Importantly, AI-ETD+ differs from other hybrid fragmentation techniques in that it does not add any additional time to the scan sequence. The IR photo-activation occurs immediately after the transfer of ions into the low pressure trap for a duration of ~4 ms. This time is typically utilized as a ion cooling time prior to mass analysis in the low pressure cell, but it is more than sufficient to create generate IRMPD products with the reduced bath gas pressure of the low pressure cell.

Figure 5 shows AI-ETD, EThcD, and AI-ETD+ spectra of the doubly protonated precursor of the synthetic peptide INQLISETEAVVTNELEDGR. Extensive fragmentation is seen for each method, and the signal in b-, c-, y, and $z^{\bullet}$-type ions is shown in bar graphs to the right. This signal is normalized to the most intense signal from all three conditions, which was y-type ion signal in AI-ETD+. The EThcD spectrum has more b- and y-type fragment ions than the AI-ETD spectrum, which is expected, but c- and $z^{\bullet}$-type products are somewhat diminished – apparent in both the spectra and the bar graphs. AI-ETD+ maintains c- and $z^{\bullet}$-type product ion signal, with even more fragments being generated than in either AI-ETD or EThcD, and it also produces substantial b- and y-type ion series with greater signal than EThcD. Far less unreacted precursor is present in the EThcD spectrum, but AI-ETD+ still has more signal in product ions channels. Note, all three spectra are on the same intensity scale, which further highlights the lower overall signal detected in EThcD spectra compared to AI-ETD and AI-ETD+ fragmentation. Several different combinations of laser powers were tested for AI-ETD+, with the best combination being 18 W for AI-ETD, followed by 9 W for the IMRPD activation in the low pressure cell. Power output from the laser is easily modulated in the instrument code on this timescale.

The benefits of AI-ETD+ from this test case translate to LC-MS/MS experiments, as well, making it the optimal supplemental activation technique for ETD. Figure 6 compares ETD, ETcaD, EThcD, AI-ETD, and AI-ETD+ fragmentation for 90-minute analyses of tryptic peptides from mouse brain lysate. Note, AI-ETD in this comparison is with a laser power of 18 W, AI-ETD+ is shown using a combination of 18W and 9W for respective activation stages, and the ETD and AI-ETD data correspond to the analyses shown in Figure 4. Table S1 provides the average and standard deviation of MS/MS scans, PSMs, unique peptides, and overall MS/MS success rate for all analyses, including multiple laser powers and laser

power combinations for AI-ETD and AI-ETD+, respectively. Note, EThcD and AI-ETD+ data were searched using c-, z$^{\bullet}$-, b-, and y-type fragments (using all four gave the best performance) while all other analyses used only c-, z$^{\bullet}$-, and y-type products for searching (Figure S4).

AI-ETD+ provides the greatest number PSMs (Figure 6a) and generally boosts MS/MS success rate the most across the *m/z* range and for lower charge state precursors (z = 2 and 3). AI-ETD+ was slightly outperformed by AI-ETD and EThcD for precursors with m/z < 500 Th (Figure 6b) and standard AI-ETD is clearly better for higher charged precursors (z ≥ 4) (Figure 6c), which are factors to keep in mind when designing future experiments. Regardless, AI-ETD or AI-ETD+ provided the best results, and AI-ETD+ doubled the overall MS/MS success rate of ETD (63.22% vs. 31.56%), while AI-ETD and EThcD nearly doubled ETD's success rate (59.96% and 58.19%, respectively). It is worth noting that even with similar success rates, AI-ETD noticeably increased PSM identifications over EThcD. This is likely because more MS/MS scans were acquired in AI-ETD analyses. AI-ETD does not slow down scan acquisition relative to standard ETD due to its concurrent activation regime, whereas EThcD requires additional time to perform the collisional activation step (Figure S5). Most interestingly, AI-ETD+ also maintained expected numbers of MS/MS scans and did not increase scan times because it utilizes time already built into the scan sequence to perform its additional IRMPD activation (Figure S5)

Beyond identification metrics, the quality of fragmentation for EThcD, AI-ETD, and AI-ETD+ was also assessed. In Figure 6d, the extent of peptide backbone sequence coverage is examined by counting the number of bond cleavages missed, *i.e.*, bonds where no fragment ion of any type was observed. If zero bond cleavages are missed, the peptide had 100% sequence coverage, or every bond could be explained by an observable fragment ion. For this comparison, PSMs for all three technical replicate injections were pooled for each fragmentation method, and only z = +2 precursors were considered since they are the majority of precursors selected and are the case were these supplemental activation methods provide the most benefit over ETD. The total numbers of PSMs (n) are provided for each fragmentation method. AI-ETD+ performs significantly better than EThcD and AI-ETD, providing 100% sequence coverage (zero bond cleavages missed) for the large majority (~85%) of PSMs identified, with another 10% having only one cleavage missed. AI-ETD sequences more PSMs with zero bond cleavages missed than EThcD, but EThcD outperforms AI-ETD when considering PSMs with zero or one missed bond cleavage. AI-ETD+ also generates the highest number of fragment ions per PSM, which is broken down by count of each of the four fragment in types in Figure 6e. Interestingly, AI-ETD+ produces more b- and y-type ions than EThcD and more c- and z$^{\bullet}$-type ions than standard AI-ETD, indicating that it is also activating some degree of ETnoD products that AI-ETD is not fully mitigating. Standard AI-ETD produces more c- and z$^{\bullet}$-type fragments than EThcD, but similar numbers of y-type fragments and fewer b-type ions. These results show promise for both AI-ETD and AI-ETD+ in standard proteomic experiments, but they also highlight the potential AI-ETD+ has to be a new hybrid fragmentation method for challenging applications like *de novo* sequencing where extensive ion series and multiple fragmentation methods are highly valuable, if not necessary.[52–54]

CONCLUSION

Enabling photo-dissociation capabilities on the newest generation of Orbitrap hybrid instruments offers many new exciting possibilities. Here we have shown how a quadrupole-Orbitrap-linear ion trap Tribrid MS system (Orbitrap Fusion Lumos) can be easily outfitted with a continuous wave CO_2 infrared laser by affixing the laser head and optics directly to the instrument chassis for a robust implementation. Moreover, we perform the first AI-ETD analyses on the Lumos platform, demonstrating that concurrent IR photo-activation during ETD substantially improves peptide fragmentation and nearly doubles identifications in LC-MS/MS of complex peptide mixtures. With the other ETD-specific improvements already afforded by the Lumos system, this work represents the state-of-the-art ETD technology for proteomic experiments. We have also introduced a new hybrid fragmentation technique called AI-ETD+ that combines AI-ETD and IRMPD fragmentation to generate extensive c/z$^{\bullet}$- and b/y-type fragment ion series in a single MS/MS spectrum without adding any time to the scan acquisition. AI-ETD+ represents the optimal supplemental fragmentation method for ETD analyses over any other approach and enables 100% sequence coverage for the large majority of identifications it generates. This work enables new directions in research for *de novo* peptide sequencing, PTM characterization, intact protein analysis, and more, and we investigate the benefits of AI-ETD for bottom-up and top-down phosphoproteomics in a companion manuscript.[55]

Supplementary Material

Refer to Web version on PubMed Central for supplementary material.

Acknowledgments

The authors gratefully acknowledge support from Thermo Fisher Scientific and NIH grant R35 GM118110 awarded to J.J.C. N.M.R. was funded through an NIH Predoctoral to Postdoctoral Transition Award (F99 CA212454). The authors also thank Jae Schwartz, John E. P. Syka, Chris Mullen, and Chad Weisbrod for helpful discussions.

References

1. Syka JEP, Coon JJ, Schroeder MJ, Shabanowitz J, Hunt DF. Proc. Natl. Acad. Sci. U. S. A. 2004; 101:9528–9533. [PubMed: 15210983]
2. Coon JJ. Anal Chem. 2009; 81:3208–3215. [PubMed: 19364119]
3. Zhurov KO, Fornelli L, Wodrich MD, Laskay Üa, Tsybin YO. Chem. Soc. Rev. 2013; 42:5014–5030. [PubMed: 23450212]
4. Prentice BM, McLuckey SA. Chem. Commun. 2013; 49:947–965.
5. Sarbu M, Ghiulai RM, Zamfir AD. Amino Acids. 2014; 46:1625–1634. [PubMed: 24687149]
6. Brodbelt JS. Anal. Chem. 2016; 88:30–51. [PubMed: 26630359]
7. Earley L, Anderson LC, Bai DL, Mullen C, Syka JEP, English AM, Dunyach J-J, Stafford GC, Shabanowitz J, Hunt DF, Compton PD. Anal. Chem. 2013; 85:8385–8390. [PubMed: 23909443]
8. Riley NM, Mullen C, Weisbrod CR, Sharma S, Senko MW, Zabrouskov V, Westphall MS, Syka JEP, Coon JJ. J. Am. Soc. Mass Spectrom. 2016; 27:520–531. [PubMed: 26589699]
9. Rose CM, Rush MJP, Riley NM, Merrill AE, Kwiecien NW, Holden DD, Mullen C, Westphall MS, Coon JJ. J. Am. Soc. Mass Spectrom. 2015; doi: 10.1007/s13361-015-1183-1
10. Good DM, Wirtala M, McAlister GC, Coon JJ. Mol. Cell. Proteomics. 2007; 6:1942–1951. [PubMed: 17673454]

11. Lermyte F, Williams JP, Brown JM, Martin EM, Sobott F. J. Am. Soc. Mass Spectrom. 2015; 26:1068–1076. [PubMed: 25862188]
12. Laszlo KJ, Munger EB, Bush MF. J. Am. Chem. Soc. 2016; 138:9581–9588. [PubMed: 27399988]
13. Pitteri SJ, Chrisman PA, McLuckey SA. Anal. Chem. 2005; 77:5662–5669. [PubMed: 16131079]
14. Liu J, McLuckey SA. Int. J. Mass Spectrom. 2012; 330:174–181. [PubMed: 23264749]
15. Clemmer DE, Hudgins RR, Jarrold MF. J. Am. Chem. Soc. 1995; 117:10141–10142.
16. Breuker K, Oh H, Horn DM, Cerda BA, McLafferty FW. J. Am. Chem. Soc. 2002; 124:6407–6420. [PubMed: 12033872]
17. Swaney DL, McAlister GC, Wirtala M, Schwartz JC, Syka JE, Coon JJ. Anal Chem. 2007; 79:477–485. [PubMed: 17222010]
18. Frese CK, Altelaar AFM, van den Toorn H, Nolting D, Griep-Raming J, Heck AJR, Mohammed S. Anal. Chem. 2012; 84:9668–9673. [PubMed: 23106539]
19. O'Connor PB, Lin C, Cournoyer JJ, Pittman JL, Belyayev M, Budnik BA. J. Am. Soc. Mass Spectrom. 2006; 17:576–585. [PubMed: 16503151]
20. Sun R-X, Dong M-Q, Song C-Q, Chi H, Yang B, Xiu L-Y, Tao L, Jing Z-Y, Liu C, Wang L-H, Fu Y, He SM. J. Proteome Res. 2010; 9:6354–6367. [PubMed: 20883037]
21. Xia Y, Han H, McLuckey SA. Anal. Chem. 2008; 80:1111–1117. [PubMed: 18198896]
22. Ledvina AR, McAlister GC, Gardner MW, Smith SI, Madsen Ja, Schwartz JC, Stafford GC, Syka JEP, Brodbelt JS, Coon JJ. Angew. Chem. Int. Ed. Engl. 2009; 48:8526–8528. [PubMed: 19795429]
23. Ledvina AR, Beauchene Na, McAlister GC, Syka JEP, Schwartz JC, Griep-Raming J, Westphall MS, Coon JJ. Anal. Chem. 2010; 82:10068–10074. [PubMed: 21062032]
24. Ledvina AR, Rose CM, McAlister GC, Syka JEP, Westphall MS, Griep-Raming J, Schwartz JC, Coon JJ. J. Am. Soc. Mass Spectrom. 2013; 24:1623–1633. [PubMed: 23677544]
25. Riley NM, Westphall MS, Coon JJ. Anal. Chem. 2015; 87:7109–7116. [PubMed: 26067513]
26. Rose CM, Russell JD, Ledvina AR, McAlister GC, Westphall MS, Griep-Raming J, Schwartz JC, Coon JJ, Syka JEP. J. Am. Soc. Mass Spectrom. 2013; 24:816–827. [PubMed: 23609185]
27. Senko MW, Remes PM, Canterbury JD, Mathur R, Song Q, Eliuk SM, Mullen C, Earley L, Hardman M, Blethrow JD, Bui H, Specht A, Lange O, Denisov E, Makarov A, Horning S, Zabrouskov V. Anal. Chem. 2013; 85:11710–11714. [PubMed: 24251866]
28. Stefely JA, Kwiecien NW, Freiberger EC, Richards AL, Jochem A, Rush MJP, Ulbrich A, Robinson KP, Hutchins PD, Veling MT, Guo X, Kemmerer ZA, Connors KJ, Trujillo EA, Sokol J, Marx H, Westphall MS, Hebert AS, Pagliarini DJ, Coon JJ. Nat. Biotechnol. 2016; 34:1191–1197. [PubMed: 27669165]
29. Hebert AS, Richards AL, Bailey DJ, Ulbrich A, Coughlin EE, Westphall MS, Coon JJ. Mol. Cell. Proteomics. 2014; 13:339–347. [PubMed: 24143002]
30. Richards AL, Hebert AS, Ulbrich A, Bailey DJ, Coughlin EE, Westphall MS, Coon JJ. Nat. Protoc. 2015; 10:701–714. [PubMed: 25855955]
31. Geer LY, Markey SP, Kowalak JA, Wagner L, Xu M, Maynard DM, Yang X, Shi W, Bryant SH. J. Proteome Res. 2004; 3:958–964. [PubMed: 15473683]
32. Wenger CD, Phanstiel DH, Lee MV, Bailey DJ, Coon JJ. Proteomics. 2011; 11:1064–1074. [PubMed: 21298793]
33. Good DM, Wenger CD, McAlister GC, Bai DL, Hunt DF, Coon JJ. J Am Soc Mass Spectrom. 2009; 20:1435–1440. [PubMed: 19362853]
34. Good DM, Wenger CD, Coon JJ. Proteomics. 2010; 10:164–167. [PubMed: 19899080]
35. Riley NM, Rush MJP, Rose CM, Richards AL, Kwiecien NW, Bailey DJ, Hebert AS, Westphall MS, Coon JJ. Mol. Cell. Proteomics. 2015; 14:2644–2660. [PubMed: 26193884]
36. Riley NM, Bern M, Westphall MS, Coon JJ. J. Proteome Res. 2016; 15:2768–2776. [PubMed: 27402189]
37. Chalkley RJ, Medzihradszky KF, Lynn AJ, Baker PR, Burlingame AL. Anal. Chem. 2010; 82:579–584. [PubMed: 20028093]

38. Coon JJ, Syka JEP, Schwartz JC, Shabanowitz J, Hunt DF. Int. J. Mass Spectrom. 2004; 236:33–42.
39. Gunawardena HP, He M, Chrisman PA, Pitteri SJ, Hogan JM, Hodges BDM, McLuckey SA. J. Am. Chem. Soc. 2005; 127:12627–12639. [PubMed: 16144411]
40. Lermyte F, Łącki MK, Valkenborg D, Baggerman G, Gambin A, Sobott F. Int. J. Mass Spectrom. 2015; 390:146–154.
41. Swaney DL, McAlister GC, Coon JJ. Nat. Methods. 2008; 5:959–964. [PubMed: 18931669]
42. Madsen JA, Cheng RR, Kaoud TS, Dalby KN, Makarov DE, Brodbelt JS. Chemistry. 2012; 18:5374–5383. [PubMed: 22431222]
43. Cannon JR, Holden DD, Brodbelt JS. Anal. Chem. 2014; 86:10970–10977. [PubMed: 25270663]
44. Shaffer CJ, Marek A, Pepin R, Slovakova K, Turecek F. J. Mass Spectrom. 2015; 50:470–475. [PubMed: 25800183]
45. Frese CK, Zhou H, Taus T, Altelaar AFM, Mechtler K, Heck AJR, Mohammed S. J. Proteome Res. 2013; 12:1520–1525. [PubMed: 23347405]
46. Mommen GPM, Frese CK, Meiring HD, van Gaansvan den Brink J, de Jong APJM, van Els CACM, Heck AJR. Proc. Natl. Acad. Sci. U. S. A. 2014; 111:4507–4512. [PubMed: 24616531]
47. Riley NM, Coon JJ. Anal. Chem. 2016; 88:74–94. [PubMed: 26539879]
48. Second TP, Blethrow JD, Schwartz JC, Merrihew GE, MacCoss MJ, Swaney DL, Russell JD, Coon JJ, Zabrouskov V. Anal. Chem. 2009; 81:7757–7765. [PubMed: 19689114]
49. Gardner MW, Smith SI, Ledvina AR, Madsen JA, Coon JJ, Schwartz JC, Stafford GC, Brodbelt JS, Brodbelt JS. Anal. Chem. 2009; 81:8109–8118. [PubMed: 19739654]
50. Ledvina AR, Lee MV, McAlister GC, Westphall MS, Coon JJ. Anal. Chem. 2012; 84:4513–4519. [PubMed: 22480380]
51. Brodbelt JS. Chem. Soc. Rev. 2014; 43:2757–2783. [PubMed: 24481009]
52. Savitski MM, Nielsen ML, Kjeldsen F, Zubarev RA. J. Proteome Res. 2005; 4:2348–2354. [PubMed: 16335984]
53. Kim S, Mischerikow N, Bandeira N, Navarro JD, Wich L, Mohammed S, Heck AJR, Pevzner PA. Mol. Cell. Proteomics. 2010; 9:2840–2852. [PubMed: 20829449]
54. Guthals A, Clauser KR, Frank AM, Bandeira N. J. Proteome Res. 2013; 12:2846–2857. [PubMed: 23679345]
55. Riley NM, Hebert AS, Durnberger G, Stanek F, Mechtler K, Westphall MS, Coon JJ. Anal. Chem. 2017 *in press*.

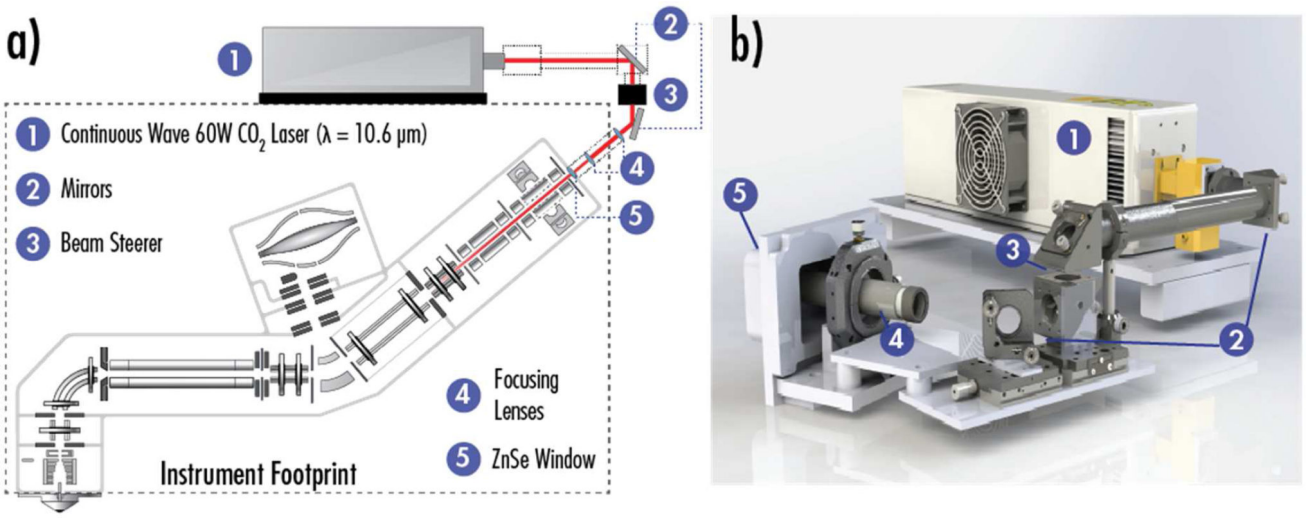

Figure 1. Instrument modifications for Activated Ion Electron Transfer Dissociation (AI-ETD)

a) An instrument schematic summarizes the hardware additions made to implement AI-ETD in the dual cell linear ion trap on the Orbitrap Fusion Lumos. Additions include the CO_2 laser, guiding mirrors, beam steerers, focusing lenses, and an entrance window added to the vacuum manifold. All beam guiding and manipulation is done external to the vacuum chambers of the instrument. Note, the illustration is not to scale. **b)** A more detailed depiction of the laser and associated beam guides, showing the orientation of the laser mounted to the back of the instrument chassis and how the photon beam is brought concentric to the trapping volume of the linear ion trap.

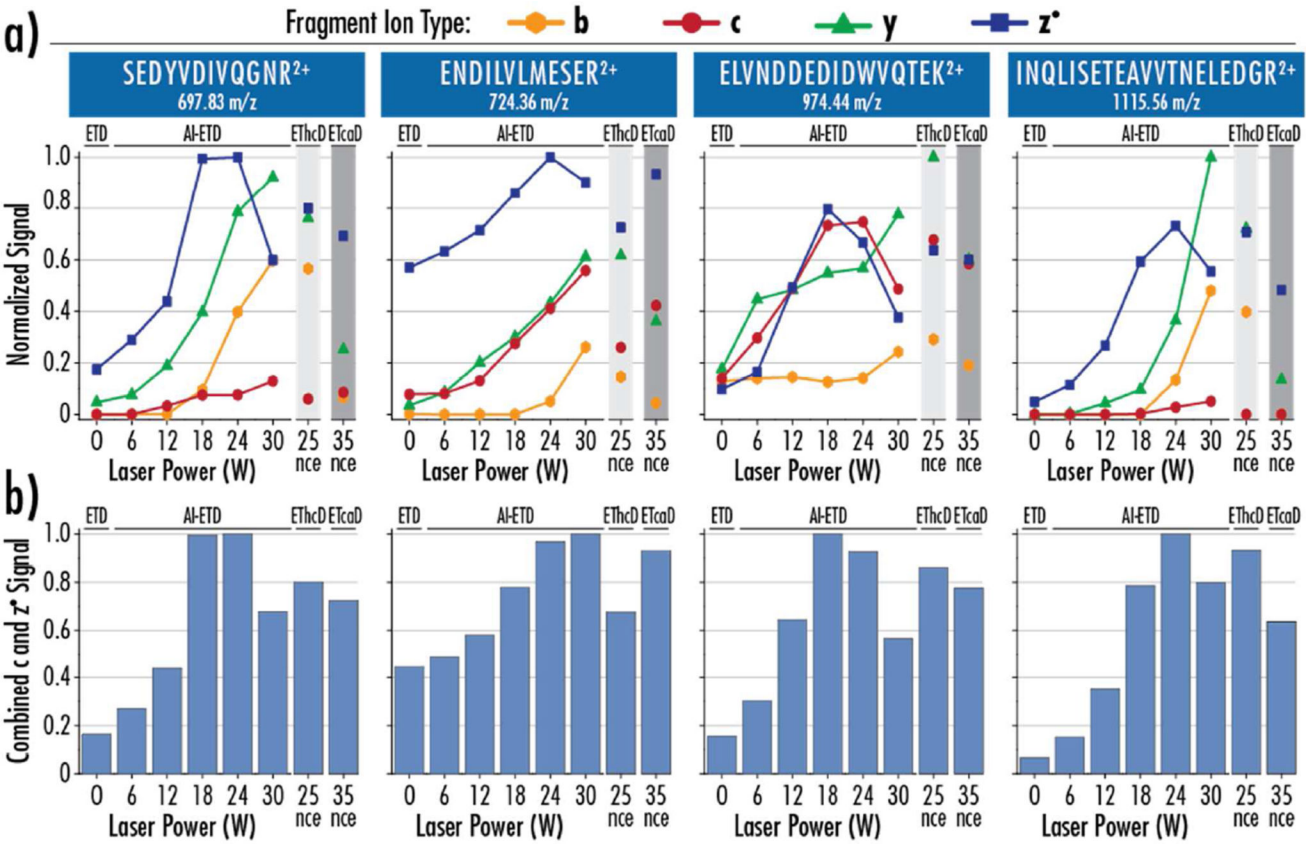

Figure 2. AI-ETD improves product ion generation over ETD, ETcaD, and EThcD

a) Increasing laser power enhances generation of *c*-, $z^{\bullet}$-, and *y*- type ions over ETD alone for four standard peptides, although too high of laser power can cause decreases in product ion intensity. Higher laser powers also begin to generate *b*-type ions, indicating onset of some degree of IRPMD. AI-ETD at 18W and 24W generally produces more product ion signal than ETcaD and EThcD supplemental activation techniques. **b)** Summing *c*- and $z^{\bullet}$-type product ion signal show how AI-ETD at varying laser powers increases ETD-specific product ions over ETD, ETcaD, and EThcD. Signal for each graph was normalized to the highest value for that condition.

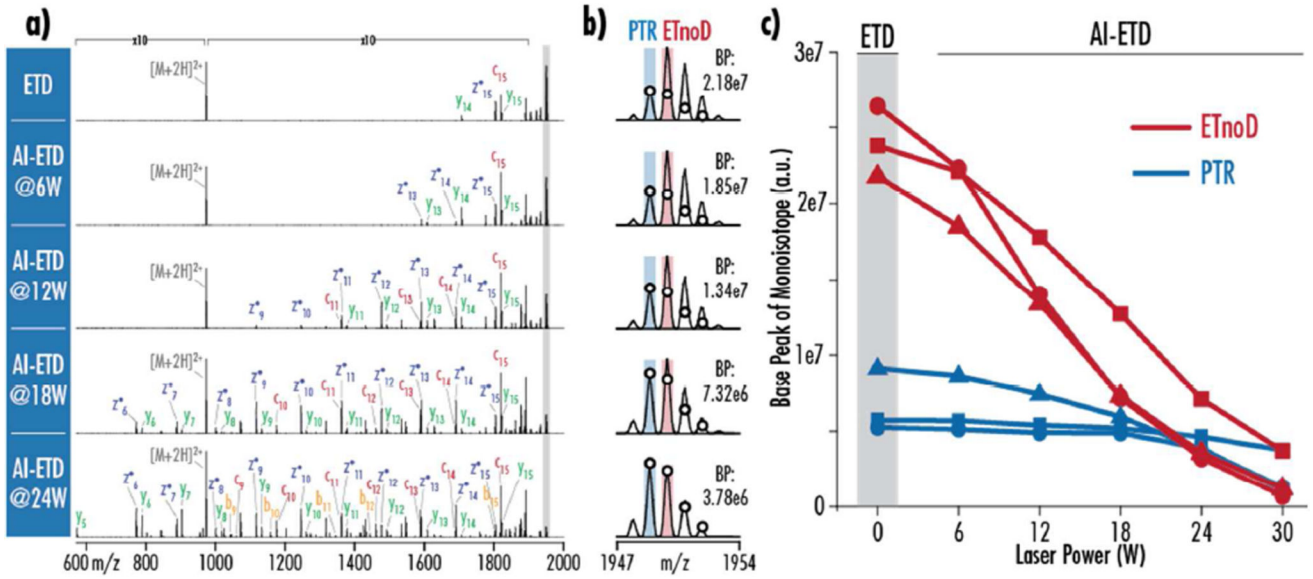

Figure 3. AI-ETD generates more product ions by decreasing ETnoD

a) Spectra from ETD and AI-ETD of increasing laser powers for the $z = +2$ precursor of ENVNDDEDIDWVQTEK show the extent to which AI-ETD can increase product in yield. All spectra are on the same intensity scale. **b)** Investigation of the charge reduced precursor products (greyed area in spectra in part a) show that the isotopic distribution shift upon AI-ETD to match the presence of PTR products only with little to no ETnoD products. Base peak intensities for each case are provided. **c)** The base peak intensity of the PTR and ETnoD monoisotopic peaks for $z = +2$ precursors of SEDYVDIVQGNR (circle), ENDILVLMESER (square), and ENVNDDEDIDWVQTEK (triangle) are plotted to show that the trend of decreasing ETnoD products with increasing AI-ETD laser power holds for each of the standard peptides. Note, the fourth peptide had a charge reduced precursor *m/z* above 2000 Th and was thus excluded from this analysis.

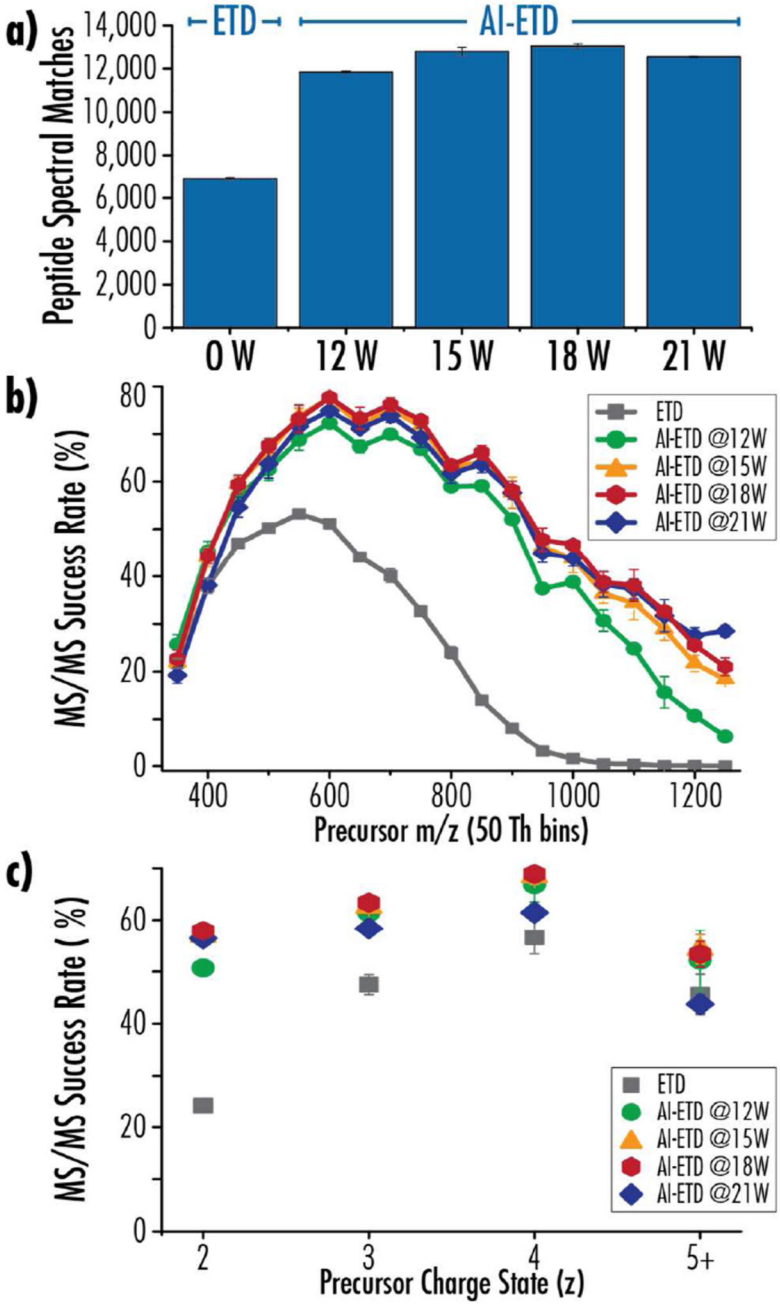

Figure 4. AI-ETD at different laser powers compared to ETD for shotgun proteomics

a) AI-ETD across a range of laser powers improves peptide identification over ETD, with AI-ETD at 18W generating the most peptide spectral matches – nearly doubling the identifications obtained from ETD alone. **b)** AI-ETD increases MS/MS success rate over ETD across the *m/z* range, especially >600 Th. **c)** AI-ETD improves MS/MS success rates over ETD for precursors of all charge states, with the exception of AI-ETD at 21W for $z \geq 5$ (5+ indicates $z \geq 5$). In general, AI-ETD at 18W performs best for all metrics. Note, success rate is defined as number of MS/MS scans successfully converted to PSMs, and all data here

represent the average of three technical replicates with one standard deviation shown by error bars.

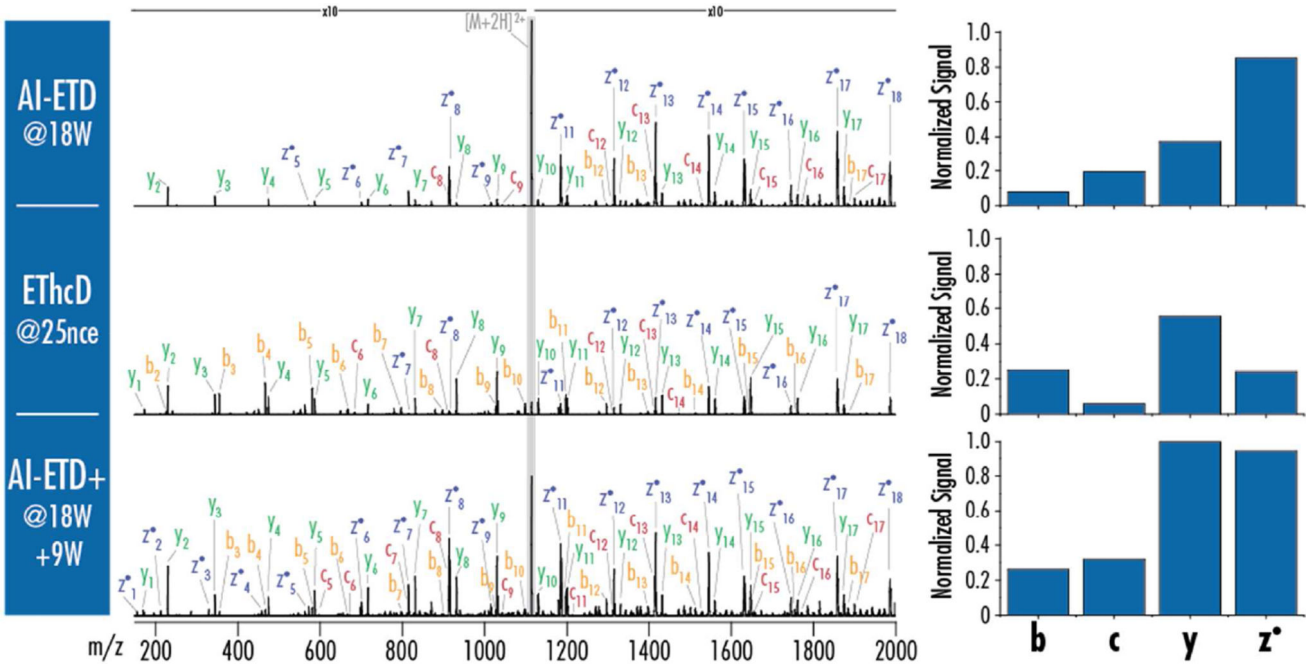

Figure 5. AI-ETD+ offers maximal generation c-, z-, b- and y-type fragments

AI-ETD+ is the combination of irradiating ions in the high pressure trap concurrent with the ETD reaction and providing a second short irradiation during product ion analysis in the low pressure trap. This scheme does not increase the overall acquisition time per scan but provides the combination of benefits of AI-ETD fragmentation plus extra collisional excitation via IRMPD immediately prior to mass analysis. Spectra for the $z = +2$ precursor of INQLISETEAVVTNELEDGR are shown for AI-ETD at 18W, EThcD with a collision energy of 25nce, and AI-ETD+ (18W during the ETD reaction and 9W during product ion analysis). AI-ETD+ maintains the *c*- and $z^{\bullet}$-type product ion signal generated by AI-ETD and also provides more *b*- and *y*-type product ion signal than EThcD. Spectra are on the same intensity scale, and product ion signals were normalized to the highest value across all three conditions.

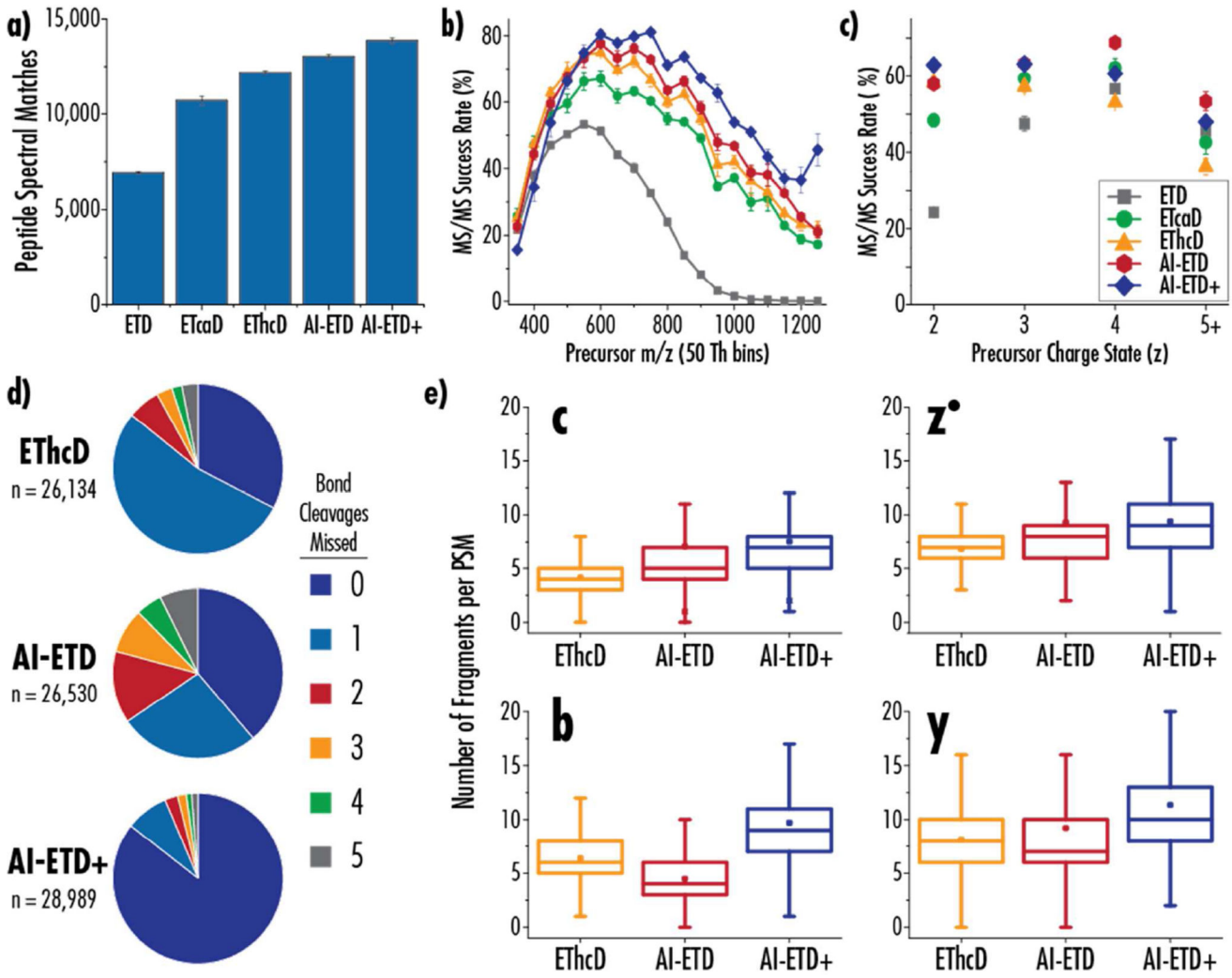

Figure 6. AI-ETD+ is the optimal supplemental activation technique for shotgun proteomic analyses

a) Peptide spectral matches for ETD and four different ETD supplemental activation methods are shown, with AI-ETD+ providing the best identification power. MS/MS success rates for precursor *m/z* **(b)** and charge state **(c)** are also provided for each method. Note, data in a), b), and c) represent the average of three technical replicates, and error bars show one standard deviation. **d)** The number of missing bond cleavages is shown for the $z = +2$ precursors from EThcD, AI-ETD, and AI-ETD+. Zero missed cleavages indicates that 100% peptide sequence coverage was achieved for that PSM. **e)** Box plots show the distribution of total *c*-, $z^{\bullet}$, *b*-, and *y*-type product ions generated in a given PSM of $z = +2$ precursors for EThcD, AI-ETD, and AI-ETD+. Note, data in d) and e) represent the aggregate total of PSMs from all three technical replicates.